Available online at www.sciencedirect.com
ScienceDirect
International Journal of Pharmaceutics 340 (2007) 143–152
INTERNATIONAL JOURNAL OF PHARMACEUTICS
www.elsevier.com/locate/ijpharm

Pharmaceutical Nanotechnology

Transport of stavudine, delavirdine, and saquinavir across the blood–brain barrier by polybutylcyanoacrylate, methylmethacrylate-sulfopropylmethacrylate, and solid lipid nanoparticles

Yung-Chih Kuo *, Fu-Lung Su

Department of Chemical Engineering, National Chung Cheng University, Chia-Yi 62102, Taiwan, ROC

Received 14 October 2006; received in revised form 9 January 2007; accepted 7 March 2007
Available online 12 March 2007

Abstract

Permeability of the anti-human immunodeficiency virus (HIV) agents, including stavudine (D4T), delavirdine (DLV), and saquinavir (SQV), across the in vitro blood–brain barrier (BBB) was studied. Here, the anti-HIV agents were incorporated with polybutylcyanoacrylate (PBCA) nanoparticles (NPs), methylmethacrylate-sulfopropylmethacrylate (MMA-SPM) NPs, and solid lipid nanoparticles (SLNs). Transport of the anti-HIV agents across BBB is a key factor in their applications to the therapy of the acquired immunodeficiency syndrome (AIDS). Experimental results revealed that the drug order of the loading efficiency (LE) on PBCA and MMA-SPM was D4T > DLV > SQV. For the entrapment efficiency (EE) in SLNs, this order was reversed. Also, LE of D4T on MMA-SPM was larger than that on PBCA; however, the reverse was true for DLV and SQV. As the particle size increased, LE decreased and EE increased. For a fixed drug carrier, an increase in the particle size yielded a decrease in the BBB permeability coefficient of the anti-HIV agents. Moreover, enhancement in the BBB permeability was on the carrier order of PBCA > MMA-SPM > SLNs for D4T, and for DLV and SQV, the order became PBCA > SLNs > MMA-SPM. PBCA, MMA-SPM, and SLNs were efficacious carriers of D4T, DLV, and SQV to meliorate BBB permeability by 3–16 folds, indicating the clinical potential of the present NP formulations for the AIDS treatment.

Keywords: Polybutylcyanoacrylate; Methylmethacrylate-sulfopropylmethacrylate; Solid lipid nanoparticle; Blood–brain barrier; Anti-HIV agent; AIDS

1. Introduction

The central nervous system (CNS) of a vertebrate is protected by a particular tissue structure, named as the blood–brain barrier (BBB) (Scherrmann, 2002). BBB sustains the CNS homeostasis via the important roles in shunning the invasions of neurological toxins and microorganisms (Enanga et al., 2002). On the other hand, curative agents may not achieve effective concentrations in the brain owing to BBB. For the therapy of the acquired immunodeficiency syndrome (AIDS), drug transport across BBB is a crucial issue because human immunodeficiency virus (HIV) can immigrate to and multiply in CNS, yielding several neurological disorders. Moreover, HIV dwells in the brains, as suggested by the huge quantities of unintegrated HIV-1 DNA in brain tissues of the AIDS patients (Pang et al., 1990). Hence, to reduce HIV infection and inhibit viral replication, it is inevitable to produce desired therapeutic effect by delivering the anti-HIV agents across BBB. Besides, when the anti-HIV agents across the blood–cerebrospinal barrier and BBB, it was often observed that the efflux was much larger than the influx. Thus, BBB is a strict transport restriction against the anti-HIV agents.

Stavudine (D4T), delavirdine (DLV), and saquinavir (SQV) are, respectively, the typical nucleoside reverse transcriptase inhibitor, non-nucleoside reverse transcriptase inhibitor, and protease inhibitor for the AIDS treatment. In an investigation on in vitro T-lymph cells, it was concluded that D4T could yield high suppression of the function of HIV reverse transcriptase with low bone-marrow toxicity (Riddler et al., 1995). DLV, which was not involved in the viral metabolic pathways,

* Corresponding author. Tel.: +886 5 272 0411x33459; fax: +886 5 272 1206.
E-mail address: chmyck@ccu.edu.tw (Y.-C. Kuo).

0378-5173/$ – see front matter © 2007 Elsevier B.V. All rights reserved.
doi:10.1016/j.ijpharm.2007.03.012

could block the enzymatic activity of HIV-1 to avoid transcribing messages of the ribonucleic acid into the deoxyribonucleic acid (Tran et al., 2001). SQV was similar to the precursor peptides of newly developed virion buds, and could link up viral protease to hinder the proliferation of HIV-1 and HIV-2 with a very low affinity to the human protease (Gerald, 2003). Nevertheless, D4T was relatively hydrophilic, and the molecular weights of DLV and SQV were high. These caused extremely low penetrated concentration of D4T, DLV, and SQV in the brain.

For CNS-targeted delivery, five possible mechanisms were proposed (Lapin, 1996; Shah et al., 1989). However, the prevalent routes for the transport of anti-HIV agents across BBB were the passive diffusion and the carrier-mediated system (Xiaoling and William, 1999). It is worth to note that the carrier-mediated systems, including antibodies (Pardridge et al., 1991), liposomes (Huwyler et al., 1996), and colloids (Kreuter, 2001), are efficacious in the BBB transport. Especially, colloidal nanoparticles (NPs) have been concluded as effectual carriers for elevating drug concentration in the brain, although the definite transport pathways of the drug-loaded NPs have not been fully ascertained. For polymeric particles, nanoparticulate polybutylcyanoacrylate (PBCA) was capable of D4T loading (Kuo, 2005) and transport of zidovudine and lamivudine (Kuo and Chung, 2005). Nonetheless, homogeneous NPs commonly led to low loading capacities for hydrophilic pharmaceuticals (Harmia et al., 1986). Thus, for better affinity of the carriers to drugs and targeted cells, alkylmethacrylate was copolymerized with styrene or acrylic acid derivatives, such as acrylamide and acrylic acid butyl ester, to synthesize inhomogeneous NPs. For example, methylmethacrylate (MMA) and sulfopropylmethacrylate (SPM) were copolymerized to become NPs with permanent charge. MMA-SPM NPs could promote the drug-loading capacity (Langer et al., 1997) and the BBB permeability (Kuo and Chen, 2006). Furthermore, solid lipid nanoparticles (SLNs) could carry doxorubicin across BBB (Ballabh et al., 2004; Fundrao et al., 2000) and enhance bioavailability by extending the drug residence time in plasma (Bargoni et al., 1998). SLNs were also eligible carriers for the brain delivery of injected camptothecin (Yang et al., 1999). Hence, for the AIDS treatment, transport of D4T, DLV, and SQV incorporated with PBCA, MMA-SPM, and SLNs across BBB became a critical scheme. This was performed in this study.

For in vitro culture, endothelia have been isolated from tissues such as epididymis, adrenal cortex, human preputial skin, retinal microvessel, and large blood vessels (aorta, umbilical cord vein, and pulmonary artery). However, only brain-microvascular endothelial cells (BMECs) were appropriate for the BBB studies (Betz and Goldstein, 1978). In the present study, the in vitro BBB model was constituted by a culture of confluent human BMECs (HBMECs) on a microporous polycarbonate (PC) membrane. D4T, DLV, and SQV were incubated with freshly synthesized PBCA and MMA-SPM NPs to allow equilibrium loading. The three drugs were entrapped by SLNs during particulate fabrication. Permeability of D4T-, DLV-, and SQV-carrying PBCA NPs, MMA-SPM NPs, and SLNs was estimated by the drug concentration in receiver chamber of the transport system.

2. Materials and methods

2.1. Reagents and chemicals

HBMECs, endothelial cell medium (ECM), endothelial cell growth supplement (ECGS), fetal bovine serum (FBS), and penicillin/streptomycin solution (P/S) were purchased from Biocompare (South San Francisco, CA, USA). Rat tail collagen, human fibronectin, trypsin–EDTA, gelatin, anti-human von Willebrand factor VIII, anti-rabbit IgG with fluorescein isothiocyante (FITC) conjugate, ammonim persulfate (APS), dextran 70,000, L-A-phospatidylcholine type II-S, taurocholate sodium, cholesteryl hemisuccinate, mannite, D-trehalose dehydrate, D4T, FITC-dextran 70,000, 3-(4,5-dimethyl thiazol-2-yl)-2,5-diphenyl-tetrazolium bromide (MTT), MTT solubilization solution, [^{14}C]sucrose (46.6 mCi/mmol), and Dulbecco's phosphate-buffered saline (DPBS) were obtained from Sigma (St. Louis, MO, USA). Methyl methacrylate (MMA) and tripalmitin were purchased from Fluka (Buchs, Switzerland). Dimethyl sulfoxide (DMSO) was obtained from J.T. Baker (Phillipsburg, NJ, USA), Triton-X-100 from Acros (Geel, Belgium), anti-ZO-1 from Zymed (South San Francisco, CA, USA), methanol from Mallinckrodt Baker (Phillipsburg, NJ, USA), butylcyanoacrylate (BCA) from Sicomet (Sichel Werk, Germany), sulfopropyl methacrylate (SPM) from Aldrich (Milwaukee, WI, USA), *n*-butanol from Riedel-de Haën (Seelze, Germany), cacao butter from OCG Cacao (Whitinsville, MA, USA), DLV from Biomol Research (Plymouth Meeting, PA, USA), SQV from United States Pharmacopeial (Rockville, MD, USA), polysorbate 80 from FisherScientific (Fair Lamn, NJ, USA), acetonitrile (ACN) from BDH (Poole, England), human fibronectin-coated culture dish from BD Bioscience (Franklin Lakes, NJ, USA), and PC membrane (Millicell® sterilized insert) from Millipore (Bedford, MA, USA).

2.2. Cultivation and characterization of HBMECs

HBMECs were cultured on human fibronectin-coated dish in ECM, containing 5% FBS, 1% P/S, and 1% ECGS, in a humidified 37 °C, CO_2 incubator (NuAire, Plymouth, MN, USA). ECM was replaced after first 6 h and then replaced every 2 days. After 6-day cultivation, HBMECs were washed by DPBS, severed by 0.4 mL of 0.025% trypsin–0.5 mM EDTA, and equally distributed into three dishes. For the passages beyond six, gelatin-coated culture dish was employed. Excess HBMECs were frozen with ECM, containing 10% FBS and 10% DMSO, in an ultra-low temperature freezer (Sanyo, Osaka, Japan) for 1 day and then stored in liquid nitrogen. HBMECs could be unfrozen within 1 min in 37 °C water bath. HBMECs of passage 6–16 with a confluent monolayer were used in the present in vitro BBB model. Pretreatment of rat-tail collagen and human fibronectin on PC membranes was described previously (Kuo and Chung, 2005). HBMECs were seeded on the pretreated PC membrane with a density of 6×10^4 cells/cm^2, and cultivated over 14 days in the CO_2 incubator with the rate of ECM replacement of every 2 days. For immunohistochemical staining, HBMECs were seeded on 18 mm cover slip with pre-coated rat-tail collagen

of 50 μg/cm^2 and human fibronectin of 10 μg/cm^2. After cultivation, HBMECs were dehydrated in 1.5 mL of methanol. Desiccated HBMECs were treated with 1.5 mL of DPBS containing Triton-X-100 to improve the membrane permeability. HBMEC film was incubated with 1.5 mL of DPBS containing anti-human von Willebrand factor VIII, and then incubated with 1.5 mL of DPBS containing anti-rabbit IgG with FITC conjugate in the CO_2 incubator. For tight junction (TJ) characterization, 1.5 mL of 10% (v/v) formalin solution was applied, and the fixed HBMEC layer was dipped in 1.5 mL of DPBS containing anti-ZO-1. Fluorescent images of HBMECs and TJ were observed using argon laser and FITC filter at 458 nm (excitation) and 488 nm (emission) under a phase contrast fluoromicroscope (Axioskop 2 plus, Zeiss, Munchen-Hallbergmoos, Germany).

2.3. Fabrication and characterization of drug-incorporated NPs

Nanoparticulate PBCA and MMA-SPM were synthesized by the method described previously (Kuo, 2005) with minor modifications. Briefly, 0.1% (v/v) BCA was added into an acidic medium containing 0.1% (w/v) dextran 70,000 at 25 °C over a pre-specified reaction span. Polymerization was terminated by neutralization of 0.1N NaOH. In the presence of APS, 0.05% (w/v) SPM was copolymerized with 4.95% (v/v) MMA at 78 °C over 24 h. MMA-SPM NP suspension was filtrated through a filter paper. PBCA NP suspension and white MMA-SPM NP filtrate were purified by centrifugation at 5100 × *g* for 10 min, refrigerated at −80 °C in the ultra-low temperature freezer for 30 min, and lyophilized (Eyela, Tokyo, Japan) over 36 h in the presence of 4% (w/v) mannitol.

Loading of D4T, DLV, and SQV on NPs was achieved by the method described previously (Kuo, 2005) with minor modifications. Concisely, 0.1% (w/v) D4T, DLV, or SQV was mixed with 0.6% (w/v) lyophilized PBCA or MMA-SPM NPs in DPBS. Drugs were allowed to be adsorbed in equilibration onto the NP carriers in a baths-reciprocal shaker at 150 rpm and 37 °C over 3 h. D4T-, DLV- or SQV-loaded NPs were stabilized by 0.04% (relative to the total volume of suspension) polysorbate 80 and equilibrated at 150 rpm and 37 °C over 30 min. The drug-loaded, polysorbate 80-filmed NP suspension was ultracentrifuged by an Eppendorf centrifuge (5415D, Eppendorf AG, Hamburg, Germany) at 11,500 × *g* over 1 h. Loading efficiency was evaluated by high performance liquid chromatography (HPLC, Jasco, Tokyo, Japan) with a UV–vis spectrophotometer (UV-2075 Plus, Jasco) at 244 nm for D4T, 211 nm for DLV, and 239 nm for SQV. Mobile phase, containing ACN gradient from 5 to 45% over 20 min with a fluid flow rate of 0.85 mL/min, was driven by two high pressure pumps (PU-2080 Plus, Jasco) in series.

SLNs entrapping D4T, DLV or SQV were prepared by the method described previously (Kuo and Lin, 2006) with several modifications. In brief, 4% (w/v) tripalmitin, 3% (w/v) cacao butter, 0.5% (w/v) drug, 7% (w/v) phospatidylcholine, 4.5% (w/v) cholesteryl hemisuccinate, 9.2% (v/v) *n*-butanol, and 2.4% (w/v) taurocholate were mixed at 70 °C and 300 rpm. The microemulsion was slowly added into deionized water at 2 °C and 1200 rpm for 15 min with the final volume ratio of 1:10. SLN suspension was filtrated through a filter paper and centrifuged at 14,000 × *g* over 30 min. The supernatant was analyzed by the HPLC-UV system, and pellet was resuspended with 2% (w/v) trehalose, refrigerated at −80 °C in the −80 °C freezer over 30 min, and lyophilized. Note that the weight ratio of drug to polymeric nanoparticles or lipid phase, *r*, was also a significant parameter for drug carriage. Loading efficiency (LE) and entrapment efficiency (EE) of D4T, DLV, or SQV were defined as follows:

$$\text{LE or EE} = \frac{\text{total weight of drugs} - \text{weight of free drugs}}{\text{total weight of drugs}} \times 100\%$$

Particle size distribution of the drug-loaded NPs and the drug-entrapped SLNs was analyzed by a zetasizer 3000 HS_A with photo correlation spectroscopy (Malvern, Worcs, UK). Infrared absorption spectra were obtained by a Fourier-transform infrared spectrometer (FTIR, Shimadzu, Columbia, MD, USA).

2.4. Interaction between NPs and HBMECs

Fluorescent PBCA, MMA-SPM, and SLNs were synthesized by FITC-conjugated dextran as stabilizer, loading agent, and entrapping material, respectively. HBMECs were incubated in ECM containing 0.01% (w/v) FITC-labeled particles over 66 min. Specific staining for the cytoplasmic fluorescence using anti-human von Willebrand factor VIII and anti-rabbit IgG with FITC conjugate was employed. Fluorescent images of particle uptake by HBMECs were obtained through a phase contrast fluoromicroscope.

For estimation of the trans-endothelia electrical resistance (TEER) and the cytotoxicity, HBMECs with a density of 6×10^4 cells/cm^2 were seeded on pretreated PC membranes in a 12-well tissue culture plate. ECM containing 0.25% (w/v) particles was applied to the culture for 2 h. TEER of HBMEC monolayer was determined by the Millicell electrical resistance system (Millipore). HBMECs and 1.2 mL of MTT was incubated for 12 h. After removal of MTT and addition of 1.2 mL of MTT solubilization solution in complete darkness, the yellowish solution became purplish blue. Two hundred microliters of solution was detected by a UV–vis spectrophotometer (Bio-Tek Instruments, Winooski, VT, USA) at 570 nm.

2.5. NPs-incorporated permeability of D4T, DLV, and SQV across HBMECs

The in vitro BMEC transport system was described previously (Kuo and Chung, 2005) with the replacement of bovine BMECs by HBMECs. Briefly, circulated 37 °C water was employed in the exterior jacket of donor and receiver chambers. Moderate magnetic stirring was used at the bottom middle of the both horizontal chambers for uniformly distributed NP–drug complex in the medium. For SLN carriers, 50 μL of sample were drawn out from the receiver every 10 min, dissolved in 450 mL of methanol, and analyzed by HPLC followed a UV–vis spectrophotometer. The total medium volume in the receiver chamber was immediately compensated by 50 μL of fresh assay DPBS when sampling. After 2 h, 10 mL of receiver sample were ultra-

centrifuged at 11,500 × *g*, and the supernatant fluid was detected by the HPLC-UV system. [^{14}C]Sucrose (0.5 μCi) served as a paracellular transport marker to ascertain the confluence of the HBMEC monolayer. Radioactivity in samples of the permeability study was determined by a scintillation counter (Beckman, Palo Alto, CA, USA). The permeability coefficient of D4T, DLV, and SQV across HBMECs, P_{HBMECs}, was calculated by

$$\frac{1}{P_{HBMECs}} = \frac{1}{P_e} - \frac{1}{P_m}$$

$$P_i = \frac{J}{\Delta C} = V_r \frac{(dC_r/dt)}{(A \times \Delta C)}, \quad i = e \text{ or } m$$

where P_e, P_m, J, ΔC, and V_r are, respectively, the permeability across PC membrane with HBMECs, the permeability across PC membrane, the mass flux from donor into receiver, the concentration difference between donor and receiver, and the volume of receiver.

3. Results and discussion

3.1. Incorporation of D4T, DLV, and SQV with PBCA, MMA-SPM, and SLNs

FTIR spectra of NPs with and without drug are presented in Fig. 1. As revealed in spectrum (a) of Fig. 1(I), the main functional groups of PBCA NPs were C–O, 1250 cm^{-1}, C=O, 1750 cm^{-1}, and C≡N, 2200 cm^{-1}, which were consistent with the literature results (Sullivan and Birkinshaw, 2004). Since D4T, DLV, and SQV contained C–N, C=C, and N–H groups, absorptions of the three functional groups were observed, respectively, at 1100, 1650, and 3500 cm^{-1} for the drug-loaded PBCA NPs, as exhibited in spectra (b–d) of Fig. 1(I). As shown in spectrum (a) of Fig. 1(II), C–O, C=O, S–O, and S=O groups in MMA-SPM NPs were detected. This spectrum was consistent with the chemical structure of copolymerized MMA-SPM compound (Kuo, 2005; Langer et al., 1996). Absorptions of C–N, C=C, and N–H groups were also found for the drug-loaded MMA-SPM NPs, as displayed in spectra (b–d) of Fig. 1(II). Fig. 1(I and II) suggests that D4T, DLV, and SQV were physically adsorbed on PBCA or MMA-SPM surfaces. As indicated in spectrum (a) of Fig. 1(III), C–O, C=C, and C=O groups in pure tripalmitin SLNs were observed. Besides tripalmitin absorptions, OH group in cacao butter was examined, as presented in spectrum (b) of Fig. 1(III). As suggested in spectra (c–e) of Fig. 1(III), absorptions of C–N and N–H groups were identified for the drug-entrapped SLNs. These results suggested that loading or entrapment of the three drugs by the three carriers was successful.

Table 1 lists LE of D4T, DLV, and SQV on PBCA and MMA-SPM NPs. LE of D4T for $r = 8.3\%$ were close to 100%. As indicated in this table, the larger the particle, the lower LE for a specific drug and a fixed r. For a constant average diameter and a fixed r, LE of the three drugs followed the order of D4T > DLV > SQV. For a specific drug and a constant average diameter, a large r leaded to a low LE. LE of D4T on MMA-SPM NPs was larger than that on PBCA NPs. On the contrary, LE of

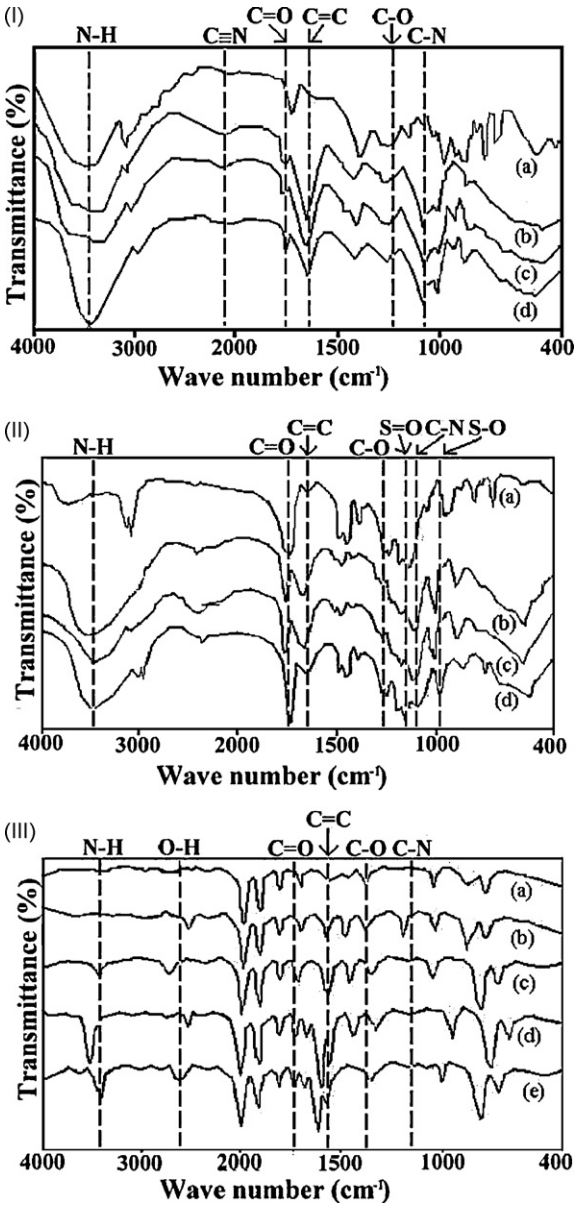

Fig. 1. FTIR spectra of the drug–carrier complexes: (I) PBCA NPs, (II) MMA-SPM NPs, and (III) SLNs. For (I and II), $r = 16.7\%$ and (a) pure carriers, (b) D4T-loaded system, (c) DLV-loaded system, and (d) SQV-loaded system. For (III), $r = 7.14\%$ and (a) tripalmitin SLNs, (b) tripalmitin and cacao butter (T-CB) SLNs, (c) D4T-entrapped T-CB SLNs, (d) DLV-entrapped T-CB SLNs, and (e) SQV-entrapped T-CB SLNs.

DLV and SQV on PBCA NPs was larger than that on MMA-SPM NPs. Monodispersed carriers were favorable to the homogeneity of drug loading, entrapment, and transport (Kuo, 2005). During manufacture, the polymeric carriers were fabricated first, and then D4T, DLV, or SQV were added into the NP suspension for adsorption on the particle surfaces. The polymer surfaces possessed lipophilic groups, and dextran 70,000 on the carrier surfaces as a stabilizer also supplied the hydrophilic sites for drug loading (Miyazaki et al., 2006). Also, the main factor influencing the amount of physical adsorption was the adsorption area provided by the NPs. A larger particle provided less surface area per unit mass, rendering fewer lipophilic/hydrophilic

Table 1
Loading efficiency of D4T, DLV, and SQV

	r^a = 8.3%		r^a = 16.7%		
	DLV	SQV	D4T	DLV	SQV
D^b of PBCA (nm)					
92.4	98.1 ± 0.98	94.4 ± 2.83	67.6 ± 4.73	38.8 ± 2.71	33.3 ± 1.66
127	94.7 ± 1.89	88.7 ± 3.55	59.0 ± 2.36	36.3 ± 1.82	30.1 ± 1.81
134	92.0 ± 3.68	80.6 ± 4.83	57.0 ± 2.85	32.6 ± 1.89	26.4 ± 2.37
184	82.3 ± 4.12	70.5 ± 5.64	50.2 ± 3.52	29.1 ± 2.62	19.2 ± 1.92
D^b of MMA-SPM (nm)					
7.7	90.4 ± 1.81	33.2 ± 1.99	86.2 ± 4.31	32.4 ± 2.60	12.0 ± 1.44
12.7	89.3 ± 2.68	31.3 ± 2.51	84.3 ± 1.69	32.0 ± 3.20	9.85 ± 4.93
44.4	88.8 ± 3.55	27.5 ± 3.58	75.1 ± 3.01	30.4 ± 1.52	7.25 ± 0.72
67.5	88.2 ± 4.41	25.0 ± 2.00	71.3 ± 4.28	29.1 ± 1.75	5.54 ± 0.55

[a] r denotes the weight ratio of drug to nanoparticles.
[b] D is the average diameter of nanoparticles.

surface groups per unit mass (Guicheux et al., 1997). For a suspension of constant carrier amount, larger carriers resulted in fewer total loading sites (Horstmann et al., 1986). Hence, larger PBCA and MMA-SPM particles produced lower LE. In the case of a low r, freely suspended drugs adhered to PBCA or MMA-SPM surfaces by strong attraction of the vacant sites. Thus, a low r yielded a high LE. For a fixed size of PBCA and MMA-SPM, LE of the three drugs was on the order of D4T > DLV > SQV. This order is opposite to the order of molecular weight: D4T (224.2) < DLV (516.0) < SQV (670.7) and the logarithm of octanol/buffer partition coefficient (log D_{oct}): D4T (−0.72) < DLV (2.98) < SQV (4.51). The rationale behind the order was that a small drug molecule with a weak hydrophobicity was advantageous to the adsorption onto the hydrophilic PBCA and MMA-SPM surfaces.

Fig. 2(I and II) shows, respectively, the variation in the average diameter of SLNs as a function of the drug–lipid weight ratio and the variation in EE as a function of the average diameter of SLNs. The differences between the present SLNs and the previously fabricated SLNs (Kuo and Lin, 2006) included an increase in the content of cacao butter and the entrapment of the three anti-HIV agents in the internal lipid cores. Note that cacao butter is easily biodegradable and very biocompatible. For a specific drug, the average diameter of SLNs increased with the drug–lipid weight ratio, as exhibited in Fig. 2(I). The order of entrapped drugs on the increase in SLN diameter was SQV > DLV > D4T, in general. As indicated in Fig. 2(II), EE increased with the average diameter of SLNs for a specific drug. EE of the three drugs was generally on the order of SQV > DLV > D4T. Note that the order of EE in SLNs was the same as the order of log D_{oct} of the three drugs. This is because the internal lipid phase of SLNs was efficient to the entrapment of hydrophobic drugs.

3.2. Uptake of PBCA, MMA-SPM, and SLNs by HBMECs

Morphology of the current HBMECs was characterized by specific binding to the polyclonal first antibody followed by the fluorescein-labeled secondary antibody (Jaffe et al., 1973). Specific binding to the monoclonal first antibody was employed for the TJ staining (Rao et al., 2002). To demonstrate the applicability of the present BBB system, interaction between HBMECs and the three drug carriers were identified by the

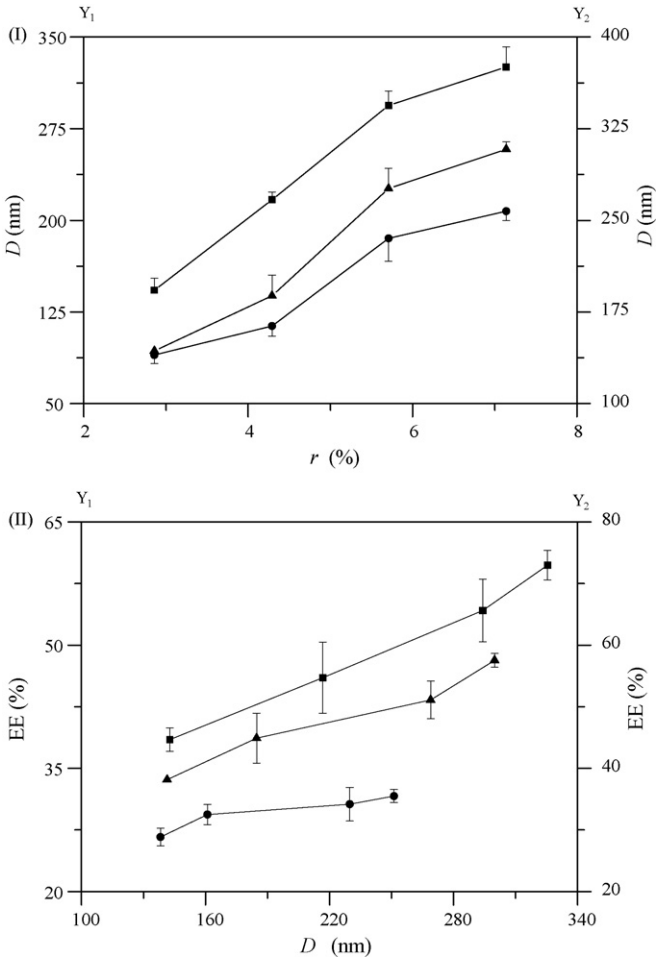

Fig. 2. (I) Effect of the weight ratio of drug to lipid phase, r, on the average diameter of SLNs. (Key) 7% (w/v) lipid; circles for D4T using Y_2 axis; triangles for DLV using Y_2 axis; squares for SQV using Y_1 axis. (II) Entrapment efficiency of drug in SLNs. (Key) same as Fig. 2(I).

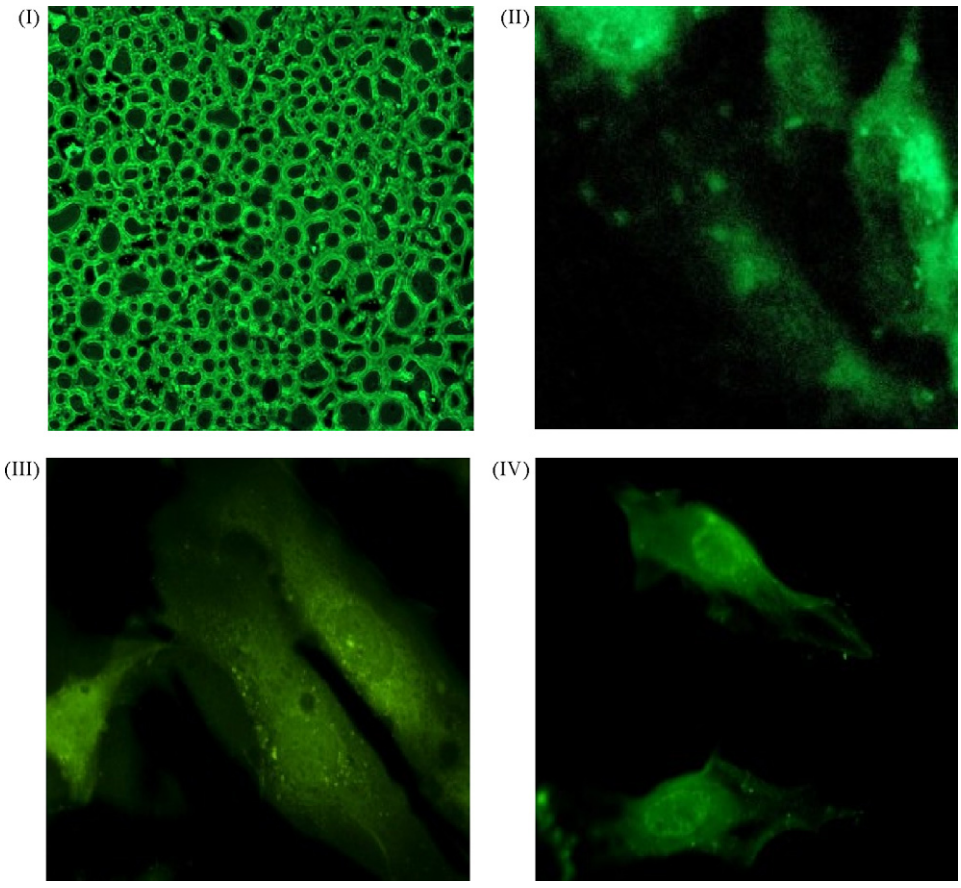

Fig. 3. Immunofluorescent images of (I) tight junction among HBMECs, (II) uptake of PBCA NPs, (III) uptake of MMA-SPM NPs, and (IV) uptake of SLNs.

immunohistochemical fluorescent staining. Here, anti-human von Willebrand factor VIII was applied to the recognition of endothelial cytoplasmic proteins in order to show the fluorescent contour of HBMECs. The results of immunochemical staining are displayed in Fig. 3. The spiderweb-like fluorescence was the contact zone among HBMECs, as exhibited in Fig. 3(I). The unstained circular regions were HBMECs. Fig. 3(I) demonstrated that the confluent monolayer of HBMECs with appropriate TJ feature was developed. As presented in Fig. 3(II–IV), the bright green spots were the FITC-labeled drug carriers, which penetrated into the cytoplasm of HBMECs. Under the same dose of NPs and the same period of treatment, intensity of the fluorescent dots for the three carriers was on the order of PBCA NPs > SLNs > MMA-SPM NPs. Note that affinity of NPs to HBMECs followed the NPs' surface-charge properties because HBMECs were negatively charged. PBCA, SLNs, and MMA-SPM carried, respectively, positive charge, medium negative charge, and strong negative charge, i.e., the order of the zeta potential was PBCA > SLNs > MMA-SPM (Kuo and Lin, 2006). Hence, the increase in the monolayer conductance followed the order of MMA-SPM > SLNs > PBCA.

3.3. Viability and TEER of HBMECs

Variation in the viability of HBMECs as a function of the average diameter of carriers is shown in Fig. 4. As implied in this figure, little cytotoxicity of the three particulate carriers was obtained. As compared with large particles, small particles were slightly toxic. Fig. 4 suggested that PBCA NPs, MMA-SPM NPs, and SLNs were exceedingly biocompatible materials with HBMECs. Cytotoxicity of the drug carriers arose mainly from the direct contact of NPs with the cell membranes or

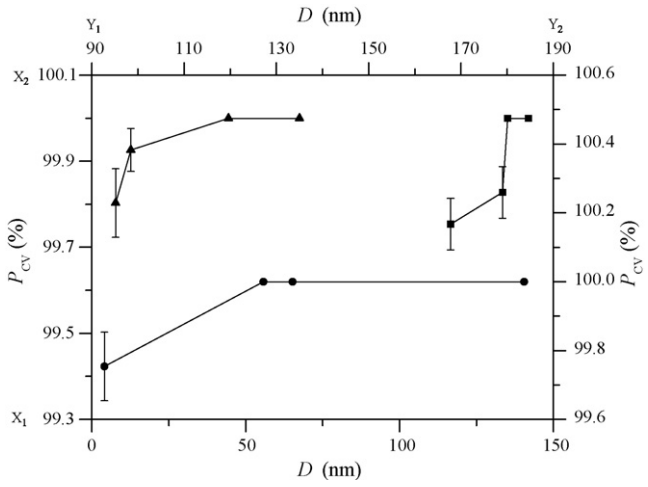

Fig. 4. HBMEC viability after the delivery of the drug carriers. Circles for PBCA NPs using X_2 and Y_2 axes; triangles for MMA-SPM NPs using X_1 and Y_1 axes; squares for SLNs using X_1 and Y_1 axes.

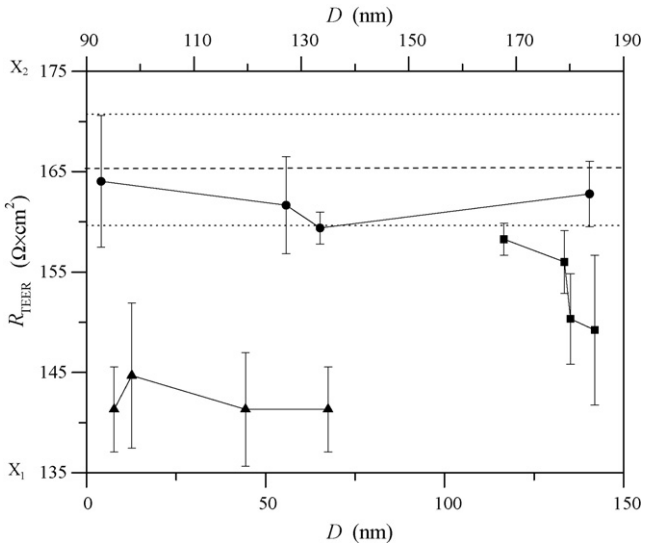

Fig. 5. Trans-endothelia electrical resistance (TEER) of the carrier-treated HBMEC monolayer. Long dash line for the average TEER and short dash line for the standard deviation without carriers; circles for PBCA NPs using X_2 axis; triangles for MMA-SPM NPs using X_1 axis; squares for SLNs using X_1 axis.

the release of inflammatory mediators by particulate irritation (Vauthier et al., 2003). Toxicity of polymeric compounds of short alkyls was higher than that of long alkyls (Müller et al., 1990). Alkyls in smaller particles were normally shorter. Furthermore, HBMEC contact frequency of small particles was higher than that of large particles. Thus, smaller particles yielded higher cytotoxicity. However, the cellular viability remained high for the case of small NPs because the NP degradation rate was slow.

Fig. 5 shows the variation in TEER as a function of the average diameter of particles. The order of the three carriers on the TEER reduction was MMA-SPM NPs > SLNs > PBCA NPs, as presented in this figure. The variation in TEER was nearly not influenced by the particle size of PBCA NPs and MMA-SPM NPs. For SLNs, TEER decreased as the average diameter increased. During the isolation of bovine BMECs (BBMECs) from finely chopped brain tissue, basement membranes and adhering pericytes were dissected by enzymatic segmentation with collagenase/dispase (Kuo and Chung, 2005). Also, cell debris and erythrocytes were discarded by Percoll gradient. However, some impurity might cause variation in the electrical resistance of the cellular monolayer. TEER of the primarily cultured BBMECs was about 150 Ω cm^2, and remained above 131 Ω cm^2 after uptake of sodium fluorescein and above 122 Ω cm^2 after uptake of FITC-labeled dextran (Gaillard and de Boer, 2000). For the present HBMEC model, TEER was about 165 Ω cm^2. After treatment of PBCA, MMA-SPM, and SLNs, TEER remained above 152, 135, and 142 Ω cm^2, respectively. The order of TEER decrease by the incorporation of the three carriers was resulted from the raise in the conductance of negative current in the HBMEC monolayer. It could also be concluded that the effect of NPs on cytotoxicity and on TEER decrease were almost independent.

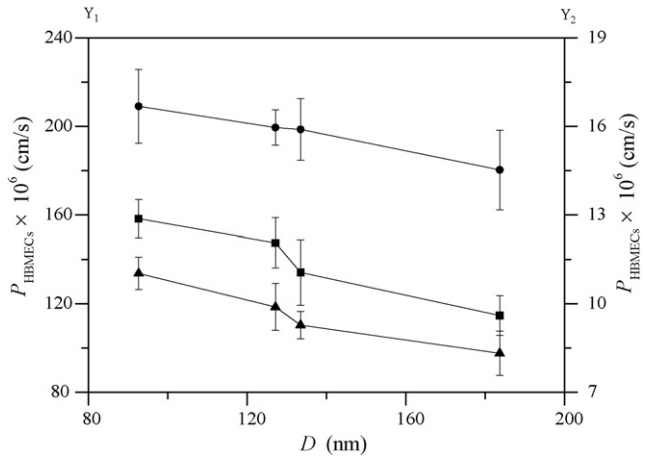

Fig. 6. Permeability coefficient of drugs across HBMEC monolayer by the drug–PBCA complex. (Key) circles for D4T using Y_1 axis; triangles for DLV using Y_2 axis; squares for SQV using Y_2 axis.

3.4. Permeability of D4T, DLV, and SQV across HBMEC monolayer

Figs. 6–8 present the variation in P_{HBMECs} as a function of the average diameter of PBCA NPs, MMA-SPM NPs, and SLNs, respectively. As displayed in the three figures, an increase in the particle size yielded a decrease in P_{HBMECs}. Since a small particle generally produced a small mass-transfer resistance, the small carriers could be easier to penetrate through the HBMEC monolayer than the large carriers (Kuo and Chung, 2005). P_{HBMECs} of DLV and SQV loaded on PBCA NPs and MMA-SPM NPs with $r = 8.3$ and 16.7% is listed in Table 2. The SLN results were not shown in this table because r influenced the SLN diameter. Thus, effect of r on P_{HBMECs} was included in Fig. 8. On the contrary, particulate diameter was almost independent of r for the two polymeric NPs. As exhibited in Table 2, little effect of r on P_{HBMECs} was concluded. P_{HBMECs} of free drug was $12.5 \pm 0.64 \times 10^{-6}$ cm/s for D4T, $0.599 \pm 0.039 \times 10^{-6}$ cm/s for DLV, and $0.739 \pm 0.059 \times 10^{-6}$ cm/s for SQV in the present study. These data were equivalent to the literature results (Glynn

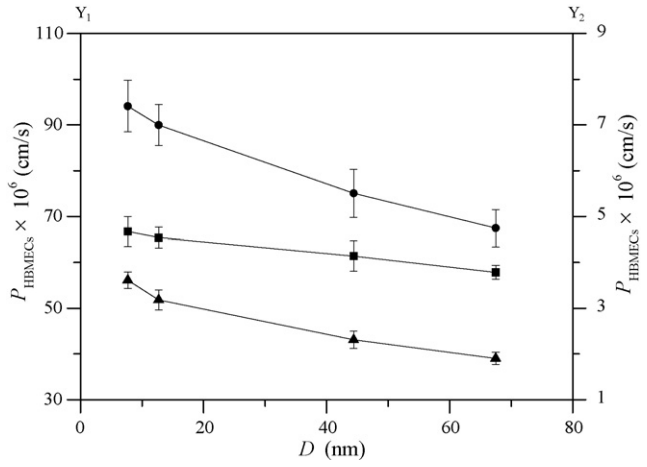

Fig. 7. Permeability coefficient of drugs across HBMEC monolayer by the drug–MMA-SPM complex. (Key) same as Fig. 6.

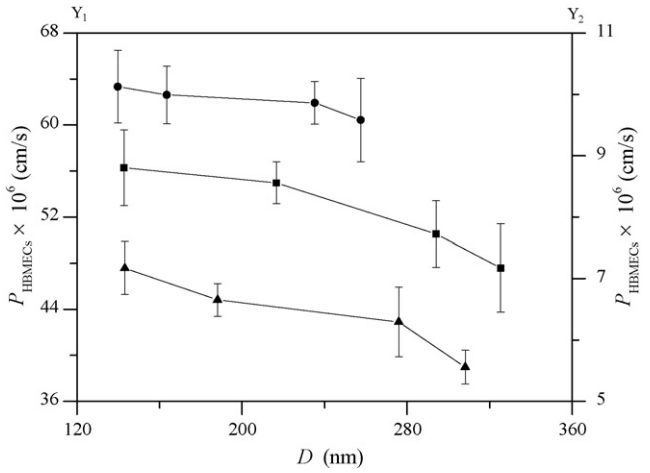

Fig. 8. Permeability coefficient of drugs across HBMEC monolayer by the drug–SLN complex. (Key) same as Fig. 6.

and Yazdanian, 1998). For the case of PBCA NPs, P_{HBMECs} was raised about 14–16 times for D4T, 12–16 times for DLV, and 12–16 times for SQV, as compared with P_{HBMECs} of free drug. For drugs loaded on MMA-SPM NPs, P_{HBMECs} became about 5–8 folds for D4T, 3–6 folds for DLV, and 4–6 folds for SQV. For drug-entrapped SLNs, increases in P_{HBMECs} were about 4–5 times for D4T, 8–11 times for DLV, and 9–11 times for SQV. For D4T, the ability of the three carriers in P_{HBMECs} enhancement was on the order of PBCA NPs > MMA-SPM NPs > SLNs. For DLV and SQV, the ability of P_{HBMECs} enhancement was on the order of PBCA NPs > SLNs > MMA-SPM NPs. Note that both the fluorescent images and the permeability results were consistent with the electrostatics. Besides, the particulate electricity increased with the SLN diameter (Cavalli et al., 2000). Large SLNs with high negative surface charge caused low drug permeability, although a large SLN carried a considerable drug amount.

The present BBB model was composed of HBMECs with TJ. Substances could pass through the barrier via either TJ (paracellular pathway) or cytoplasm (transcellular pathway) (Mullin et al., 2005). TJ, consisting of transmembrane proteins such as occludin and claudin (Hopkins et al., 2000), could not only restrain the paracellular permeability but also cause the polarized apical-basal properties of HBMECs (Abbott et al., 2006). Thus, only small water-soluble molecules could pass TJ, and transport of D4T, DLV, and SQV across BBB was mainly via the transcellular pathway. Transcellular pathway included transcellular lipophilic pathway, transport proteins, receptor-mediated transcytosis, and adsorptive transcytosis (Abbott and Romero, 1996). Due to electrostatic interaction, charged PBCA and MMA-SPM might immigrate into HBMECs via adsorptive transcytosis. Moreover, the present PBCA and MMA-SPM were coated by polysorbate 80, and the polysorbate 80-coated NPs were similar to low density lipoprotein (LDL). Therefore, NPs were recognized by membrane LDL receptors, rendering uptakes of NPs by HBMECs and drug delivery to the receiver chamber (Kreuter, 2001). Furthermore, polysorbate 80 could inhibit the efflux function of P-glycoprotein to promote the BBB penetration efficiency (Kreuter et al., 2002). The receptor-bound NPs would transport into the endothelial cytoplasm via endocytotic vesicles, which could react with lysosome to discharge the LDL receptors (Alyaudtin et al., 2001). Hence, drug was released and the receptors returned to the membrane phase. Also, apolipoprotein E (apo E), a lipoprotein fragment of LDL, was in charge of the interaction with the LDL receptors (Kreuter, 2005). Polysorbate 80 on NP surfaces could anchor apo E, rendering endocytosis of carriers by HBMECs (Weisgraber et al., 1983). Thus, polymeric NPs mimicking LDL particles may also immigrate into HBMECs via receptor-mediated transcytosis (Ramge et al., 2000; Sun et al., 2004). For drug-entrapped SLNs, contact release, membrane fusion, intermembrane transfer, and phagocytosis and endocytosis were the apt mechanisms of the BBB transport (Wissing and Müller, 2002). Membrane fusion may cause disordered SLN structure in HBMECs. However, integrity of SLN uptake by HBMECs was observed in Fig. 3(IV). Thus, the interaction between HBMECs and SLNs were not merely contact or fusion. On the other hand, drug delivery of SLN systems might also be via phagocytosis and endocytosis like polymeric NP systems, although drugs were entrapped inside the internal lipid cores. Moreover, mammalian cell membrane was composed of phospholipids, sterol, and glycolipid (Bruce et al., 2002), and the present SLNs, covered with a layer of phospatidylcholine, were similar to liposome containing phospholipids. Analogous chemical ingredient between HBMEC membranes and outer layers of SLNs might cause their interchange. Hence, intermembrane transfer would be the most prominent transport route for SLNs across the present BBB model (Vila et al., 2004).

Table 2
P_{HBMECs} (10^{-6} cm/s) of different drug–carrier ratio

Drug	r[a] (%)	PBCA[b]	MMA-SPM[c]
DLV	8.3	8.85 ± 0.367	1.86 ± 0.069
	16.7	8.27 ± 0.212	1.85 ± 0.057
SQV	8.3	9.56 ± 0.395	3.73 ± 0.142
	16.7	9.55 ± 0.308	3.74 ± 0.121

[a] r denotes the weight ratio of drug to nanoparticles.
[b] Average diameter is 184 nm.
[c] Average diameter is 68.0 nm.

4. Conclusions

Permeability of stavudine (D4T), delavirdine (DLV), and saquinavir (SQV) across the blood–brain barrier (BBB) by incorporation of polybutylcyanoacrylate (PBCA), methylmethacrylate-sulfopropylmethacrylate (MMA-SPM), and solid lipid nanoparticles (SLNs) were investigated. The loading efficiency (LE) of the three drugs on PBCA and MMA-SPM was on the order of D4T > DLV > SQV (hydrophilic order). Since MMA-SPM bore strong fixed charge, LE of D4T on MMA-SPM was larger than that on PBCA. The reverse was true for DLV and SQV. Moreover, LE decreased with an increase in the particle size. The order of the entrapment efficiency (EE) of the three drugs in SLNs followed SQV > DLV > D4T, indicating SLNs as efficient carriers for hydrophobic drugs. Also, EE increased with

the SLN diameter. The permeability of the three drugs enhanced about 12–16 folds on PBCA, 3–7 folds on MMA-SPM, and 4–11 folds in SLNs. For DLV and SQV, the order of permeability promotion was PBCA > SLNs > MMA-SPM; for D4T, PBCA > MMA-SPM > SLNs. Through the present BBB model, the three carriers were demonstrated as constructive colloidal drug delivery systems.

Acknowledgement

This work is supported by the National Science Council of the Republic of China.

References

Abbott, N.J., Rönnbäck, L., Hansson, E., 2006. Astrocyte–endothelial interactions at the blood–brain barrier. Nat. Rev. Neurosci. 7, 41–53.

Abbott, N.J., Romero, I.A., 1996. Transporting therapeutics across the blood–brain barrier. Mol. Med. Today 2, 106–113.

Alyaudtin, R., Reichel, A., Löbenberg, R., Ramge, P., Kreuter, J., Begley, D., 2001. Interaction of poly(butylcyanoacrylate) nanoparticles with the blood–brain barrier in vivo and in vitro. J. Drug Target. 9, 209–221.

Ballabh, P., Braun, A., Nedergaard, M., 2004. Microwave effects on the nervous system. Neurobiol. Dis. 16, 1–13.

Bargoni, A., Cavalli, R., Caputo, O., Fundaro, A., Gasco, M.R., Zara, G.P., 1998. Solid lipid nanoparticles in lymph and plasma after duodenal administration to rats. Pharm. Res. 15, 745–750.

Betz, A.L., Goldstein, G.W., 1978. Polarity of the blood–brain barrier: neutral amino acid transport into isolated brain capillaries. Science 202, 225–226.

Bruce, A., Alexander, J., Julian, L., Martin, R., Keith, R., Peter, W., 2002. Molecular Biology of the Cell, fourth ed. Garland Science, New York, pp. 749–753.

Cavalli, R., Caputo, O., Gasco, M.R., 2000. Preparation and characterization of solid lipid nanospheres containing paclitaxel. Eur. J. Pharm. Sci. 10, 305–309.

Enanga, B., Burchmore, R.J.S., Stewart, M.L., Barrett, M.P., 2002. Sleeping sickness and the brain. Cell. Mol. Life Sci. 59, 845–858.

Fundrao, A., Cavalli, R., Bargoni, A., Vighetto, D., Zara, G., Gasco, M.R., 2000. Non-stealth and solid lipid nanoparticles (SLN) carrying doxorubicin: pharmacokinetics and tissue distribution after i.v. administration to rats. Pharm. Res. 42, 337–343.

Gaillard, P.J., de Boer, A.G., 2000. Relationship between permeability status of the blood–brain barrier and in vitro permeability coefficient of a drug. Eur. J. Pharm. Sci. 12, 95–102.

Gerald, K.M., 2003. American Hospital Formulary Service Drug Information. American Society of Hospital Pharmacists, Bethesda, pp. 698–706.

Glynn, S.L., Yazdanian, M., 1998. In vitro blood–brain barrier permeability of nevirapine compared to other HIV antiretroviral agents. J. Pharm. Sci. 87, 306–310.

Guicheux, J., Grimandi, G., Trécant, M., Faivre, A., Takahashi, S., Daculsi, G., 1997. Apatite as carrier for growth hormone: in vitro characterization of loading and release. J. Biomed. Mater. Res. 34, 165–170.

Harmia, T., Speiser, P., Kreuter, J., 1986. Optimization of pilocarpine loading onto nanoparticles by sorption procedures. Int. J. Pharm. 33, 45–54.

Hopkins, A.M., Li, D., Mrsny, R.J., Walsh, S.V., Nusrat, A., 2000. Modulation of tight junction function by G protein-coupled events. Adv. Drug Deliv. Rev. 41, 329–340.

Horstmann, B.J., Kenny, C.N., Chase, H.A., 1986. Adsorption of proteins on sepharose affinity adsorbents of varying particle size. J. Chromatogr. 361, 179–190.

Huwyler, J., Wu, D., Pardridge, W.M., 1996. Brain drug delivery of small molecules using immunoliposomes. Proc. Natl. Acad. Sci. U.S.A. 93, 14164–14169.

Jaffe, E.A., Nachman, R.L., Becker, C.G., Minick, C.R., 1973. Culture of human endothelial cells derived from umbilical cord veins: identification by morphologic and immunologic criteria. J. Clin. Invest. 52, 2745–2756.

Kreuter, J., 2005. Application of nanoparticles for the delivery of drugs to the brain. Int. Congr. Ser. 1277, 85–94.

Kreuter, J., Shamenkov, D., Petrov, V., Ramge, P., Cychutek, K., Claudia, K.B., Alyautdin, R., 2002. Apoliporotein-mediated transport of nanoparticles-bound drugs across the blood–brain barrier. J. Drug Target. 10, pp. 371–325.

Kreuter, J., 2001. Nanoparticulate systems for brain delivery of drugs. Adv. Drug Deliv. Rev. 47, 65–81.

Kuo, Y.C., Chen, H.H., 2006. Effect of nanoparticulate polybutylcyanoacrylate and methylmethacrylate-sulfopropylmethacrylate on the permeability of zidovudine and lamivudine across the in vitro blood–brain barrier. Int. J. Pharm. 327, 160–169.

Kuo, Y.C., Lin, T.W., 2006. Electrophoretic mobility, zeta potential, and fixed charge density of bovine knee chondrocytes, methylmethacrylate-sulfopropylmethacrylate, polybutylcyanoacrylate, and solid lipid nanoparticles. J. Phys. Chem. B 110, 2202–2208.

Kuo, Y.C., 2005. Loading efficiency of stavudine on polybutylcyanoacrylate and methylmethacrylate-sulfopropylmethacrylate copolymer nanoparticles. Int. J. Pharm. 290, 161–172.

Kuo, Y.C., Chung, C.Y., 2005. Transport of zidovudine- and lamivudine-loaded polybutylcyanoacrylate and methylmethacrylate-sulfopropylmethacrylate nanoparticles across the in vitro blood–brain barrier: characteristics of the drug-delivery system. J. Chin. Inst. Chem. Eng. 36, 627–638.

Langer, K., Stieneker, F., Lambrecht, G., Mutschler, E., Kreuter, J., 1997. Methylmethacrylate sulfopropylmethacrylate copolymer nanoparticles for drug delivery. II: arecaidine propargyl ester and pilocarpine loading and in vitro release. Int. J. Pharm. 158, 211–217.

Langer, K., Marburger, C., Berthold, A., Kreuter, J., Stieneker, F., 1996. Methylmethacrylate sulfopropylmethacrylate copolymer nanoparticles for drug delivery. I: preparation and physiochemical characterization. Int. J. Pharm. 137, 67–74.

Lapin, G.D., 1996. The EMF to BBB connection: studying the effects of electromagnetic energy on the blood–brain barrier. IEEE Eng. Med. Biol. 4, 57–60.

Miyazaki, Y., Tanaka, Y., Yakou, S., Takayama, K., 2006. In vivo drug release from hydrophilic dextran tablets capable of forming polyion complex. J. Control. Release 114, 47–52.

Müller, R.H., Lherm, C., Herbot, J., Blunk, T., Couvreur, P., 1990. In vitro model for the degradation of alkylcyanoacrylate nanoparticles. Biomaterials 11, 590–595.

Mullin, J.M., Agostino, N., Erika, R.H., Thornton, J.J., 2005. Keynote review: epithelial and endothelial barriers in human disease. Drug Discov. Today 10, 395–408.

Pang, S., Koyangi, Y., Miles, S., Wiley, C., Harry, V., Chen, I., 1990. High levels of unintegrated HIV-1 DNA in brain tissue of AIDS dementia patients. Nature 34, 85–89.

Pardridge, W.M., Buciak, J.L., Friden, P.M., 1991. Selective transport of an anti-transferrin receptor antibody through the blood–brain barrier in vivo. J. Pharmacol. Exp. Ther. 259, 66–70.

Ramge, P., Unger, R.E., Oltrogge, J.B., Zenker, D., Begly, D., Kreuter, J., Briesen, H.V., 2000. Polysorbate-80 coating enhances uptake of polybutylcyanoacrylate (PBCA)-nanoparticle by human and bovine primary brain capillary endothelial cells. Eur. J. Neurosci. 12, 1931–1940.

Rao, R., Basuroy, S., Rao Jr., V.U., Karnaky, K.J., Gupta, A., 2002. Tyrosine phosphorylation and dissociation of occluding ZO-1 and E-cadherin β-catenin complexes from the cytoskeleton by oxidative stress. Biochem. J. 368, 471–481.

Riddler, S.A., Anderson, R.E., Mellors, J.W., 1995. Antiretroviral activity of stavudine. Antiviral Res. 27, 189–203.

Scherrmann, J.M., 2002. Drug delivery to brain via blood–brain barrier. Vasc. Pharmacol. 38, 349–354.

Shah, M.V., Audus, K.L., Borchardt, R.T., 1989. The application of bovine brain microvessel endothelial-cell monolayers grown onto polycarbonate membranes in vitro to estimate the potential permeability of solutes through the blood–brain barrier. Pharm. Res. 6, 624–627.

Sullivan, C.O., Birkinshaw, C., 2004. In vitro degradation of insulin-loaded poly(*n*-butylcyanoacrylate) nanoparticles. Biomaterials 25, 4375–4382.

Sun, W., Xie, C., Wang, H., Hu, Y., 2004. Specific role of polysorbate 80 coating on the targeting of nanoparticles to the brain. Biomaterials 25, 3065–3071.

Tran, J.Q., Gerber, J.G., Kerr, B.M., 2001. Delavirdine clinical pharmacokinetics and drug interactions. J. Clin. Pharm. 40, 207–226.

Vauthier, C., Dubernet, C., Fattal, E., Patrick, C., 2003. Poly(alkylcyanoacrylates) as biodegradable materials for biomedical applications. Adv. Drug Deliv. Rev. 55, 519–548.

Vila, A., Levchenko, V.V., Korytowski, W., Girotti, A.W., 2004. Sterol carrier protein-2-facilitated intermembrane transfer of cholesterol- and phospholipids-derived hydroperoxides. Biochemistry 43, 12592–12605.

Weisgraber, K.H., Innerarity, T.L., Harder, K.J., Mahley, R.W., Milnes, R.W., Marcel, Y.L., Sparrow, J.T., 1983. The receptor-binding domain of human apolipoprotein E: monoclonal antibody inhibition of binding. J. Biol. Chem. 258, 12348–12354.

Wissing, S.A., Müller, R.H., 2002. Solid lipid nanoparticles as carrier for sunscreens: in vitro release and in vivo skin penetration. J. Control. Release 81, 225–233.

Xiaoling, L., William, K.C., 1999. Transport, metabolism and elimination mechanisms of anti-HIV agents. Adv. Drug Deliv. Rev. 39, 81–103.

Yang, S.C., Lu, L.F., Cai, Y., Zhu, J.B., Liang, B.W., Yang, C.Z., 1999. Body distribution in mice of intravenously injected camptothecin solid lipid nanoparticles and targeting effect of brain. J. Control. Release 59, 299–307.